

Phason-Driven Diversity of Nucleation Pathways in Icosahedral Quasicrystals

Gang Cui,¹ Lei Zhang,² Pingwen Zhang,^{3,4} An-Chang Shi,⁵ and Kai Jiang¹

¹⁾Hunan Key Laboratory for Computation and Simulation in Science and Engineering,

Key Laboratory of Intelligent Computing and Information Processing of Ministry of Education,
School of Mathematics and Computational Science, Xiangtan University, Xiangtan, Hunan, China,
411105.

²⁾Beijing International Center for Mathematical Research, Peking University, Beijing, 100871,
China.

³⁾Institute for Math & AI, Wuhan, Wuhan University, Wuhan, Hubei, 430072, China.

⁴⁾School of Mathematical Sciences, Peking University, Beijing, 100871, China.

⁵⁾Department of Physics and Astronomy, McMaster University, Hamilton, Canada, L8S 4M1.

(*Electronic mail: kaijiang@xtu.edu.cn)

(*Electronic mail: shi@mcmaster.ca)

(*Electronic mail: pzheng@pku.edu.cn)

(Dated: 17 February 2026)

The nucleation of quasicrystals remains a fundamental puzzle, primarily due to the absence of a periodic translational template. Here, we demonstrate that phasons—hidden degrees of freedom unique to quasiperiodic order—drive diverse nucleation pathways in icosahedral quasicrystals (IQC). Combining a Landau free-energy model with the spring pair method, we compute distinct critical nuclei and their corresponding minimum energy paths. At low temperatures, a direct, symmetry-preserving pathway dominates. In contrast, higher temperatures promote a "symmetry detour" that reduces the nucleation barrier via a lower-symmetry critical nucleus. Remarkably, while the resulting bulk IQCs exhibit distinct real-space symmetries, they remain thermodynamically degenerate with identical diffraction patterns. We resolve this paradox within the high-dimensional projection framework, showing that phason shifts modulate real-space symmetry without altering bulk thermodynamics. Our findings establish phasons as the structural origin of pathway diversity, offering a new physical picture for the emergence of quasiperiodic order.

I. INTRODUCTION

Nucleation is the pivotal event in constructing the ordered world, governing the formation of crystals, polymers, and proteins alike.^{35,58,68} While nucleation in conventional periodic crystals has been extensively studied^{17,43,60}, the nucleation mechanisms of quasicrystals (QCs) remain far less understood. QCs challenge the traditional paradigm of structural order, as they exhibit long-range order in the absence of translational periodicity⁵⁷. This aperiodic order originates from the projection of a higher-dimensional periodic lattice^{25,30,33,65}, introducing the hidden *phason* degree of freedom⁵⁹. In this framework, phasons correspond to displacements in the perpendicular hyperspace (β_{\perp})^{25,59}, appearing either as spatially varying *phason fluctuations* $\beta_{\perp}(\mathbf{r})$ or as a uniform *phason shift* with $\beta_{\perp}(\mathbf{r}) \equiv \mathbf{C}$. Phason fluctuations enable low-energy local rearrangements that can assist QC stabilization and growth^{14,23,26,36,47,54,63,66,69}. By contrast, a uniform phason shift collectively reshuffles atomic motifs, thereby altering the real-space symmetry of QCs while leaving both diffraction patterns and bulk free energy invariant^{41,67}. In the absence of any thermodynamic bias, how does nucleation kinetics break this phason-shift degeneracy and select a specific real-space symmetry variant?

Unraveling this question hinges on characterizing the *critical nucleus* (CN)—the transition state dictating the nucleation barrier and pathway selection. However, nucleation in QCs presents a fundamental puzzle, primarily due to the absence

of a periodic template to guide the initial assembly. This inherent difficulty is epitomized by icosahedral quasicrystals (IQC), which are quasiperiodic in all three dimensions, making them the archetypal system to investigate this problem. Experimentally, direct observation of the CN remains elusive due to its transient nature and extreme rarity. Consequently, existing characterizations have focused primarily on the atomic structures of stable IQCs^{62,69}. In theoretical work, existing simulations have centered on stability and self-assembly^{3,7,20,29,32,40,48–50,61}, leaving the precise calculation of CNs and minimum energy paths (MEPs, the most probable nucleation pathways¹⁹) unaddressed. While multi-stage phase transitions and CNs have been identified in 2D QCs^{70,72}, the CNs of 3D IQCs remain uncharted. Most crucially, the intrinsic relationship of nucleation with phason shifts—which govern symmetry—has largely been overlooked.

Here, we address this gap by combining a Landau free-energy model³² with the spring pair method¹⁰ to compute the CNs and MEPs for nucleation into both a reference body-centered cubic (BCC) crystal and phason-shifted IQCs. Unlike the trivial translational degeneracy of periodic crystals, global phason shifts enable multiple symmetry-distinct nucleation pathways. Specifically, we identify two classes of IQC nucleation pathways distinguished by the symmetry of the CN. We further show that temperature governs the selection of nucleation pathways by altering their respective energy barriers. At low temperatures, nucleation proceeds via a direct symmetry-preserving pathway to the ideal IQC (id-IQC) with full icosahedral symmetry. At higher temperatures, nucle-

ation follows a symmetry-detour pathway that passes through a symmetry-broken CN and yields a reduced-symmetry non-ideal IQC (nid-IQC). Together, these results establish phasons as the structural origin of nucleation pathway diversity and provide a new physical picture for the emergence of quasiperiodic order from the liquid.

II. PHASON AND SYMMETRY

This section explores how phason shifts generate thermodynamically degenerate IQC variants. These variants exhibit identical diffraction intensities yet distinct real-space symmetries, a degeneracy that gives rise to the nucleation selection problem.

A. High-Dimensional Projection Framework

IQCs lack translational periodicity in three-dimensional (3D) physical space but can be elegantly described as irrational slices of a six-dimensional (6D) periodic hypercubic lattice^{30,33}. In this framework, the density field $\varphi(\mathbf{r})$ of an IQC is

$$\varphi(\mathbf{r}) = \sum_{\mathbf{h} \in \mathbb{Z}^6} \hat{\varphi}(\mathbf{h}) e^{i(\mathbf{Ph}) \cdot \mathbf{r}}, \quad \mathbf{r} \in \mathbb{R}^3, \quad (1)$$

where $\mathbf{h} \in \mathbb{Z}^6$ are the 6D reciprocal lattice vectors, $\hat{\varphi}(\mathbf{h})$ are the Fourier coefficients. The projection matrix $\mathbf{P} \in \mathbb{R}^{3 \times 6}$ maps the 6D space to the 3D physical space and is given by

$$\mathbf{P} = \begin{bmatrix} 1 & \frac{\tau}{2} & \frac{\tau}{2} & \frac{1}{2} & 0 & 0 \\ 0 & \frac{1}{2} & -\frac{1}{2} & \frac{\tau-1}{2} & 1 & 0 \\ 0 & \frac{\tau-1}{2} & \frac{1-\tau}{2} & -\frac{\tau}{2} & 0 & 1 \end{bmatrix}, \quad (2)$$

where $\tau = (1 + \sqrt{5})/2$ is the golden ratio.

B. Phason Degrees of Freedom

The high-dimensional description includes additional degrees of freedom associated with translations in the 6D superspace. A superspace translation $\beta \in \mathbb{R}^6$ modifies the IQC density through phase shifts in the Fourier modes

$$\varphi_\beta(\mathbf{r}) = \sum_{\mathbf{h} \in \mathbb{Z}^6} \hat{\varphi}(\mathbf{h}) e^{i\mathbf{h} \cdot \beta} e^{i(\mathbf{Ph}) \cdot \mathbf{r}}. \quad (3)$$

The translation decomposes into orthogonal components $\beta = \beta_{\parallel} + \beta_{\perp}$ through the corresponding high-dimensional projectors Π_{\parallel} and Π_{\perp} .

Phonon shifts, corresponding to the parallel component β_{\parallel} , induce rigid translations in physical space. Phason shifts, corresponding to the perpendicular component β_{\perp} , are unique to quasicrystals. They change the real-space decoration through a collective rearrangement of atomic positions.

1. Thermodynamic Invariants

For an infinite bulk system, the Landau free energy is invariant under any translation β , whether it corresponds to a phonon or a phason shift. As derived from the high-dimensional thermodynamic framework, the free energy depends only on closed sums of wavevectors ($\sum \mathbf{h}_i = 0$), causing the phase factors $e^{i(\sum \mathbf{h}_i) \cdot \beta}$ to cancel out exactly. Consequently,

$$E[\varphi_\beta] = E[\varphi], \quad |\hat{\varphi}_\beta(\mathbf{h})| = |\hat{\varphi}(\mathbf{h})|. \quad (4)$$

This implies that all configurations φ_β connected by phason shifts are **thermodynamically degenerate** and exhibit identical diffraction patterns.

2. Structural Variants

Thermodynamic degeneracy does not imply identical real-space symmetry. For a given superspace translation β , the residual rotational symmetry in physical space is controlled solely by the phason shift β_{\perp} . Consider a global rotation $g \in \mathcal{I}_h$, associated with a 6D unimodular lift G . This rotation remains a symmetry of φ_β only when the phason shift satisfies the compatibility condition

$$\Pi_{\perp}(G^T \beta_{\perp} - \beta_{\perp}) \in \Pi_{\perp}(2\pi\mathbb{Z}^6). \quad (5)$$

We therefore define the residual symmetry subgroup as

$$H(\beta_{\perp}) = \left\{ g \in \mathcal{I}_h \mid \Pi_{\perp}(G^T \beta_{\perp} - \beta_{\perp}) \in \Pi_{\perp}(2\pi\mathbb{Z}^6) \right\}. \quad (6)$$

When $\beta_{\perp} = 0$, the full icosahedral group is preserved and $H(\beta_{\perp}) = \mathcal{I}_h$, which defines the id-IQC. For generic $\beta_{\perp} \neq 0$, the symmetry reduces to a proper subgroup of \mathcal{I}_h , such as C_2 , which defines nid-IQC variants.

C. The IQC Nucleation Puzzle

This framework reveals a kinetic selection problem fundamentally absent in periodic crystals, as summarized schematically in Fig. 1. Global phason shifts generate a continuous family of IQC variants that are thermodynamically degenerate yet structurally distinct in real space.

The thermodynamic degeneracy of these bulk variants implies that thermodynamics alone cannot dictate the selection of a structural variant during nucleation. Instead, phason-induced structural diversity implies that nucleation may initiate from distinct local motifs, resulting in CNs with disparate symmetries. Consequently, we investigate whether these structural differences translate into distinct nucleation barriers, thereby providing a mechanism for kinetic selection. By computing the CNs and their corresponding MEPs, we quantify this selection process across representative IQC variants.

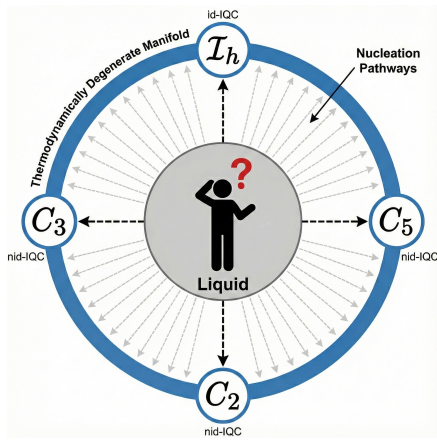


FIG. 1. **Schematic of the nucleation selection dilemma.** The liquid (center) is surrounded by a thermodynamically degenerate manifold generated by phason shifts. While these bulk states share the same free energy and diffraction intensities, they can differ in real-space symmetry, illustrated by the ideal id-IQC (\mathcal{I}_h) and representative nid-IQCs (C_5 , C_3 , C_2). Dashed arrows indicate competing kinetic routes from the liquid to different symmetry endpoints. The question mark highlights that bulk degeneracy does not determine which symmetry is selected during nucleation.

III. MODEL

The system is described by a Landau free-energy functional of a density field $\varphi(\mathbf{r})$ on a domain Ω , where $\varphi(\mathbf{r})$ denotes the deviation from a reference liquid state, and satisfies the mass-conservation constraint $\int_{\Omega} \varphi(\mathbf{r}) d\mathbf{r} = 0$. Within this framework, the free energy is given by

$$E[\varphi] = \frac{1}{2} \iint_{\Omega \times \Omega} \varphi(\mathbf{r}) G(|\mathbf{r} - \mathbf{r}'|) \varphi(\mathbf{r}') d\mathbf{r} d\mathbf{r}' + \int_{\Omega} \left(\frac{\varepsilon}{2} \varphi^2(\mathbf{r}) - \frac{\alpha}{3} \varphi^3(\mathbf{r}) + \frac{1}{4} \varphi^4(\mathbf{r}) \right) d\mathbf{r}, \quad (7)$$

where ε is a temperature-like control parameter that penalizes density fluctuations and α characterizes the intensity of three-body interaction^{5,31}. In this work, we study nucleation in a parameter regime where the homogeneous liquid $\varphi(\mathbf{r}) = 0$ is a local minimum of $E[\varphi]$, while the ordered phases of interest correspond to deeper minima.

The system is governed by an effective pair interaction potential of the Gaussian-polynomial form,

$$G(r) = \exp\left(-\frac{\sigma^2 r^2}{2}\right) \left(c_0 + c_2 r^2 + c_4 r^4 + c_6 r^6 + c_8 r^8 \right), \quad (8)$$

which has been widely used to model crystallization and quasicrystal formation^{6,32,52}.

By tuning the parameters in Eq. (8), the interaction potential stabilizes either periodic crystals with a single characteristic length scale (exemplified by the BCC phase) or IQCs involving two length scales related by the golden ratio (Fig. 2). The specific parameter sets employed in this work are carefully chosen to stabilize these distinct ordered phases.

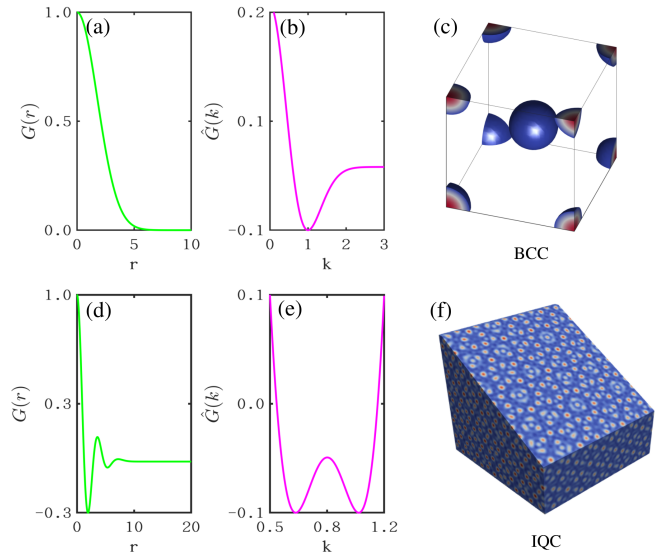


FIG. 2. **Pair interaction potentials and the ordered structures they stabilize in the present study.** (a) Real-space pair interaction potential $G(r)$ that is purely repulsive. (b) Fourier transform $\hat{G}(k)$ exhibiting a single dominant characteristic length scale. (c) The body-centered cubic (BCC) crystal stabilized by this interaction. (d) Real-space pair interaction potential $G(r)$ with alternating attractive and repulsive components (sign-changing). (e) Fourier transform $\hat{G}(k)$ exhibiting two characteristic length scales whose ratio equals the golden ratio. (f) The icosahedral quasicrystal (IQC) stabilized by this interaction.

IV. METHODS

Within the Landau free-energy framework, the undercooled liquid and ordered phases correspond to local minima of the free-energy functional $E[\varphi]$. The CN is an index-1 saddle point that separates the liquid basin from that of a given ordered phase. For each nucleation route, we characterize nucleation and subsequent growth along the associated MEP on $E[\varphi]$, and define the nucleation barrier as $\Delta E = E_{\text{CN}} - E_{\text{liq}}$.

A. Periodic Approximation Method and Discretization

To accurately simulate the nucleation of aperiodic QCs within a finite computational domain, we employ the Periodic Approximation Method (PAM)³⁴ to reduce boundary artifacts. This approach has been successfully validated for two-dimensional QC systems^{70,72}. Specifically, we approximate the IQC density field $\varphi(\mathbf{r})$ using a periodic approximant defined on a cubic domain $\Omega = [0, 2\pi L]^3$, where the integer L determines the domain size.

The approximation proceeds in two stages. First, to enforce periodicity, the projected reciprocal vectors $\lambda = \mathbf{Ph} \in \mathbb{R}^3$ (which typically have irrational components) are approximated by rational vectors $\mathbf{k}/L \in \mathbb{Q}^3$, yielding a periodic approximant

$$\varphi(\mathbf{r}) = \sum_{\mathbf{h} \in \mathbb{Z}^6} \hat{\varphi}(\mathbf{h}) e^{i\mathbf{Ph} \cdot \mathbf{r}} \approx \sum_{\mathbf{k} \in \mathbb{Z}^3} \hat{\varphi}(\mathbf{k}) e^{i\frac{\mathbf{k}}{L} \cdot \mathbf{r}}, \quad (9)$$

where $\mathbf{k} = \{\lfloor \lambda_j L \rfloor\}_{j=1}^3$, with $\lfloor x \rfloor$ denoting rounding to the nearest integer. For the IQC, the coefficients to be approximated simultaneously—derived from the elements of the projection matrix (Eq. 2)—are $\frac{1}{2}$ and $\frac{\tau}{2}$. The resulting approximation error is quantified by the Diophantine error¹³

$$E_{DA}(L) = \left\| \left(\frac{1}{2}, \frac{\tau}{2} \right) - \frac{1}{L} \left(\left\lfloor \frac{L}{2} \right\rfloor, \left\lfloor \frac{\tau L}{2} \right\rfloor \right) \right\|_{\infty}. \quad (10)$$

The local minima of E_{DA} occur at $L = 16, 26, 42, \dots$. Numerical verifications confirm that these minima with $L \geq 26$ ensure both sufficient numerical accuracy and a domain volume large enough to contain the CN. Consequently, we set $L = 26$ for all IQC simulations, yielding $E_{DA}(26) \approx 1.32 \times 10^{-3}$.

Second, for numerical implementation, we truncate the Fourier spectrum,

$$\mathbf{K}_N^3 = \left\{ \mathbf{k} \in \mathbb{Z}^3 : -\frac{N}{2} \leq k_j < \frac{N}{2}, j = 1, 2, 3 \right\}, \quad (11)$$

which yields the truncated expansion

$$\varphi(\mathbf{r}) \approx \sum_{\mathbf{k} \in \mathbf{K}_N^3} \hat{\varphi}(\mathbf{k}) e^{i\frac{\mathbf{k}}{L} \cdot \mathbf{r}}. \quad (12)$$

We discretize Eq. 12 using a Fourier pseudo-spectral method with $N = 256$ grid points in each dimension, enabling efficient evaluation of nonlinear convolution terms via the fast Fourier transform.

B. Spring Pair Method

We identify CNs by locating index-1 saddle points of the discretized free-energy functional $E[\varphi]$ using the SPM¹⁰. SPM is a gradient-only saddle-search scheme that evolves two spring-coupled replicas and converges to a saddle without Hessian evaluations, while providing an estimate of the unstable mode.

For each parameter set, we initialize SPM from the homogeneous liquid state (with small mean-zero random perturbations) and repeat the search from multiple independent initializations to sample distinct CNs. Given a converged saddle φ^* and its unstable mode \mathbf{u} , we obtain the associated MEP by relaxing $\varphi^* \pm \delta \mathbf{u}$ via gradient descent. The two downhill branches connect the liquid basin and the target ordered basin¹⁰.

C. Structural Analysis and Visualization

Particle positions are extracted as the coordinates of local maxima of the density field $\varphi(\mathbf{r})$. Structural visualization and rendering are performed using OVITO.

V. RESULTS AND DISCUSSION

A. Nucleation of BCC Crystal: A Reference Case

Before addressing IQC nucleation, we examine BCC crystallization as a reference system. For this classic periodic crystal, all thermodynamically equivalent configurations differ only by rigid translations in physical space, corresponding to phonon shifts, with no phason degrees of freedom. This makes BCC nucleation an ideal baseline for contrasting periodic and quasiperiodic ordering.

Figure 3 shows the temperature dependence of BCC nucleation. Over the entire range of ε investigated, the critical nuclei retain BCC symmetry, while their size and the associated nucleation barrier increase monotonically with temperature [Fig. 3(a,b)]. Meanwhile, the free energy of the bulk BCC phase increases with increasing temperature [Fig. 3(c)], reflecting a weakening thermodynamic driving force for crystallization, consistent with classical crystal nucleation theory. The corresponding MEP at $\varepsilon = 0.0025$ [Fig. 3(d)], typical of the entire range investigated, reveals a direct, symmetry-preserving pathway characterized by the simple accumulation of BCC unit cells.

Since the degeneracy in BCC crystals stems solely from translational symmetry, all nucleation pathways leading to thermodynamically equivalent BCC states are identical up to a rigid translation. Even if nonclassical mechanisms such as two-step nucleation^{15,39,43} occur, this translational equivalence remains unchanged.

B. Nucleation and Growth of IQCs

1. Two Distinct IQC CNs

Unlike the trivial translational degeneracy in periodic crystals, phason degrees of freedom render IQCs thermodynamically degenerate yet structurally distinct. This phason-enabled structural multiplicity may give rise to pathway diversity via symmetry-distinct CNs.

To quantify this, we computed the CNs and MEPs for nucleation from the supercooled liquid into both the id-IQC and nid-IQC. Figure 4 presents two representative pathways that reveal two symmetry-distinct classes of IQC nucleation, based on the symmetry of the CN.

In the *id-IQC nucleation pathway*, the CN consistently exhibits full icosahedral symmetry (\mathcal{I}_h) over a wide temperature range [Fig. 4(a,b)]. The atomic configuration in Fig. 4(b) confirms that the CN shares the symmetry and key structural motifs of the final id-IQC steady state. We refer to such paths as *symmetry-preserving* routes.

In contrast, the *nid-IQC nucleation pathway* proceeds through a reduced-symmetry CN. For nucleation toward a representative C_2 -symmetric nid-IQC, the CN displays pronounced pseudo-sixfold local motifs rather than icosahedral order [Fig. 4(c,d)], indicating a *symmetry-detour* route in which the CN is symmetry-mismatched with the final state.

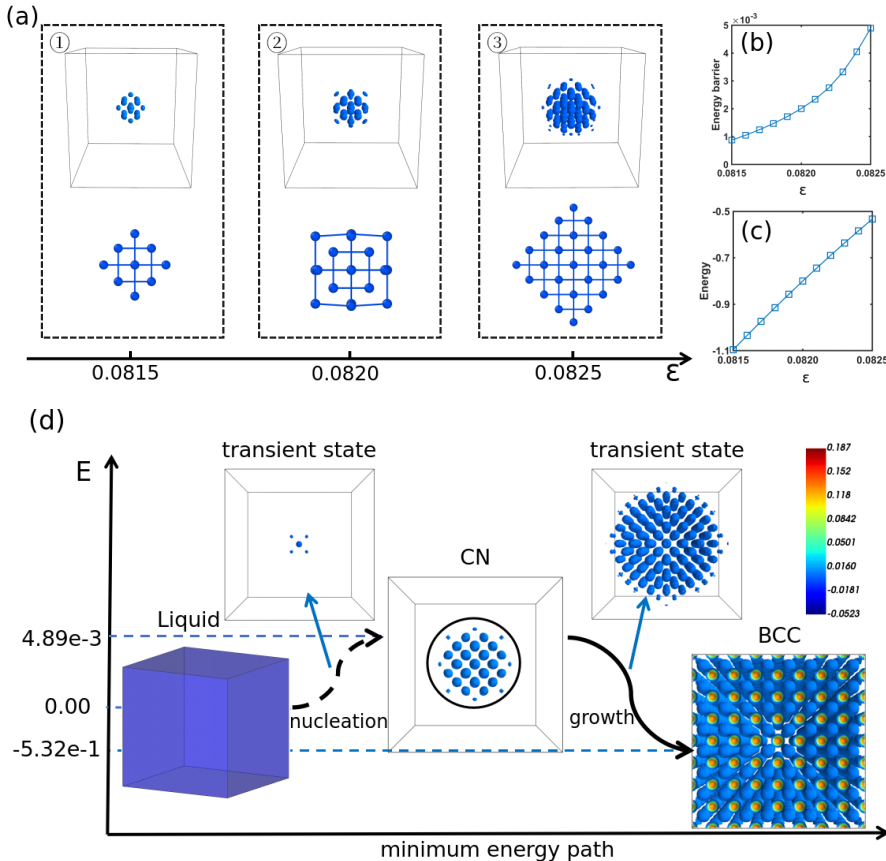


FIG. 3. Nucleation of the BCC crystal as a reference case. (a) Evolution of BCC CNs at increasing temperatures ($\varepsilon = 0.0015, 0.0020, 0.0025$; $\alpha = 0.2$). Upper panels show density distributions, and lower panels show the corresponding atomic arrangements with BCC connectivity. The CNs preserve BCC symmetry while increasing in size. (b) Nucleation energy barrier as a function of temperature. (c) Free energy of the bulk BCC phase grown from the CNs, indicating a weakening thermodynamic driving force with increasing temperature. (d) MEP for BCC nucleation and growth at $\varepsilon = 0.0025, \alpha = 0.2$.

Temperature determines pathway selection by modifying their nucleation barriers. Figure 4(e) shows a clear temperature-dependent crossover. At lower temperatures, the symmetry-preserving id-IQC pathway faces a lower barrier and is kinetically favored. However, as temperature increases, the id-IQC barrier rises steeply, leading to a crossover near $\varepsilon \approx 0.0865$. Beyond this point, the symmetry-detour nid-IQC pathway becomes the preferred kinetic route. Crucially, since the free energies of the developed id-IQC and nid-IQC bulk phases are identical [Fig. 4(f)], this selection is purely kinetic rather than thermodynamic.

The physical origin of this crossover lies in the competition between the energetic gain from ordering and the quadratic penalty for density modulations. At lower temperatures (small ε), the quadratic cost $E_f = \int_{\Omega} \frac{\varepsilon}{2} \phi^2 d\mathbf{r}$ is small, allowing the formation of a fully \mathcal{I}_h -symmetric nucleus with modest penalty. At higher temperatures, however, enforcing perfect \mathcal{I}_h symmetry necessitates high-amplitude density modulations to maintain structural order, causing E_f to rise sharply. By temporarily relaxing the symmetry constraint, the nid-IQC nucleus avoids this steep penalty, forming with weaker modulations and a lower E_f . As quantified in Fig. 5, this differential

sensitivity drives the preference for the lower-symmetry pathway at elevated temperatures.

In summary, these results demonstrate that phason degrees of freedom unlock pathway diversity unavailable to periodic crystals. Temperature selects the kinetically favored route by tuning the cost of symmetry.

2. Nucleation and Growth Process of id-IQC

Having established the kinetic selection within these two pathway classes, we now examine their distinct microscopic nucleation and growth mechanisms by analyzing the structural evolution along the MEPs.

We first focus on the *symmetry-preserving id-IQC route*. Figure 6(a) shows a representative MEP at $\varepsilon = 0.0861$, connecting the disordered liquid directly to the id-IQC steady state. Structural evolution along this path reveals a highly ordered, hierarchical assembly. As shown in Fig. 6(b), nucleation initiates from a compact seed (T1) and rapidly develops into a CN that exhibits full \mathcal{I}_h symmetry and is structurally commensurate with the final id-IQC.

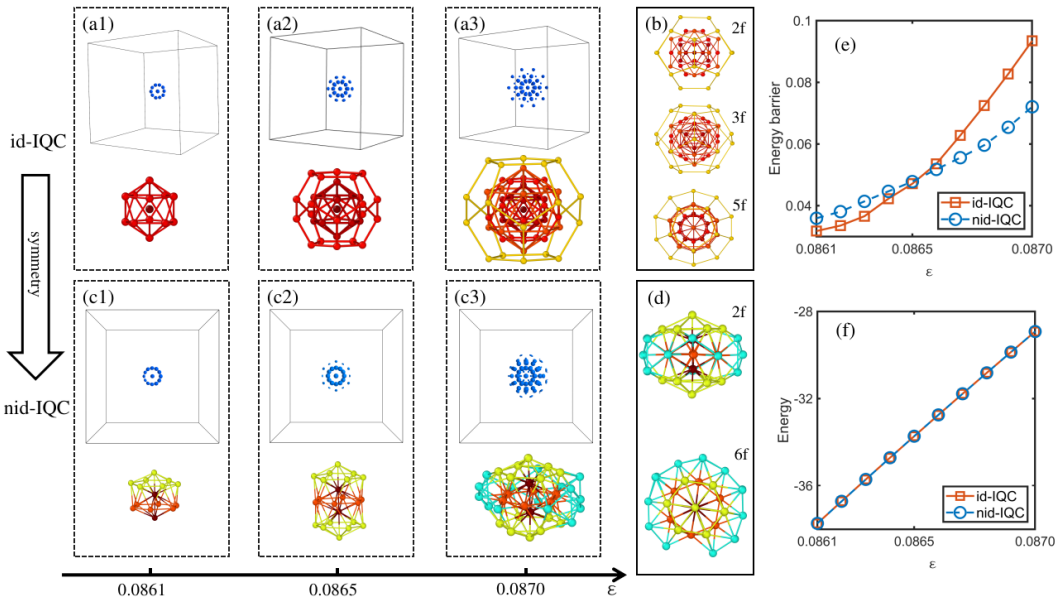


FIG. 4. Temperature-dependent CNs for id-IQC and nid-IQC and the crossover in nucleation barriers. (a1–a3) Density distributions (upper) and corresponding atomic arrangements (lower) of id-IQC CNs at $\varepsilon = 0.0861, 0.0865$, and 0.0070 ($\alpha = 0.3$), showing robust \mathcal{I}_h symmetry. (b) Atomic arrangement of (a3) viewed along 2-fold, 3-fold, and 5-fold axes, confirming full icosahedral symmetry. (c1–c3) CNs along the nid-IQC pathway at the same temperatures, exhibiting reduced symmetry with approximate 6-fold motifs. (d) Atomic arrangement of (c3) viewed along a 2-fold axis and an approximate 6-fold axis, highlighting symmetry reduction. (e) Nucleation barriers for id-IQC and nid-IQC versus ε , showing a crossover near $\varepsilon \approx 0.0865$. (f) Energies of the fully developed id-IQC and nid-IQC states versus ε , indicating degenerate thermodynamic stability.

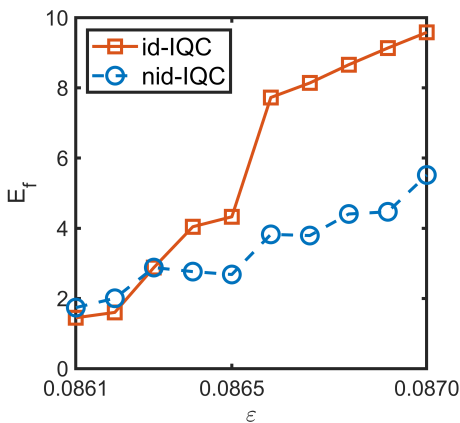


FIG. 5. Energy penalty for density fluctuations ($E_f = \int_{\Omega} \frac{\varepsilon}{2} \phi^2 dr$) in CNs as a function of temperature parameter ε for id-IQC (solid line with squares) and nid-IQC (dashed line with circles). At lower temperatures, both types of CNs exhibit similar energy penalties. However, as temperature increases, the energy penalty for id-IQC CNs rises more rapidly than for nid-IQC CNs, creating a significant energy advantage for the lower-symmetry nid-IQC nucleation pathway at higher temperatures. This demonstrates why systems preferentially form CNs with lower symmetry at elevated temperatures.

We term the subsequent growth mode “duality growth”, a mechanism that exploits the geometric duality between icosahedra and dodecahedra to maintain symmetry-preserving

growth. Specifically, dodecahedral vertices emerge along the outward normals of icosahedral faces, while new icosahedral vertices form along the normals of dodecahedral faces. This alternation preserves full \mathcal{I}_h symmetry while extending quasiperiodic order outward.

Beyond the primary shells, the growing nucleus incorporates auxiliary \mathcal{I}_h -symmetric motifs (e.g., 32-faced polyhedra and rhombicosidodecahedra at T7, T8, and T10) to fill local voids between shells, thereby improving packing and enabling the continuous extension of quasiperiodic order to the macroscopic scale.

3. Nucleation and Growth Process of nid-IQC

In stark contrast to the symmetry-preserving id-IQC route, Figure 7 details a representative *symmetry-detour pathway* leading to a C_2 -symmetric nid-IQC steady state (shown at $\varepsilon = 0.0861$). Unlike the id-IQC pathway (Figure 6), where the CN is symmetry-consistent with the final state, the nid-IQC CN is *symmetry-mismatched*. It exhibits a pronounced C_6 -symmetric character that diverges sharply from the C_2 symmetry of the eventual steady state.

Structural snapshots in Figure 7(b) reveal a “transient scaffolding” mechanism. The nucleation event establishes a C_6 -symmetric core that functions not as a permanent template, but as a temporary structural scaffold. During the intermediate growth stage (CN \rightarrow T6), this scaffold expands and consolidates, while characteristic local IQC clusters progressively

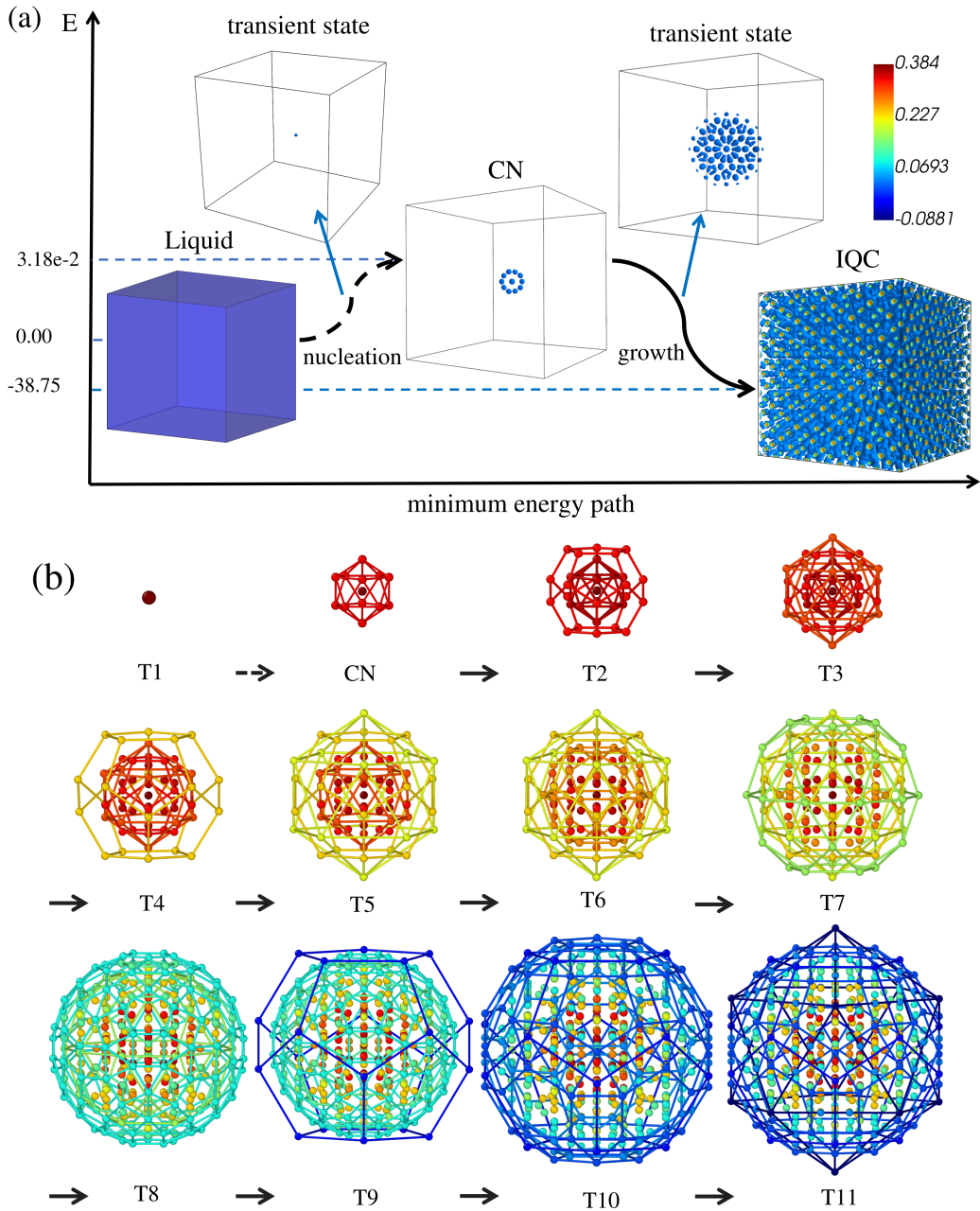


FIG. 6. Nucleation and growth process of id-IQC along the MEP at $\varepsilon = 0.0861$ and $\alpha = 0.3$. (a) MEP from the supercooled liquid (DIS) to the stable id-IQC. (b) Atomic configurations sampled along the MEP, illustrating nucleation (T1–CN) and growth (CN–T11). Particles are placed at local density maxima, with connections shown only for the three outermost layers for clarity. Colors encode the radial distance from the nucleus center (inner to outer). Nucleation starts from a small seed (T1) and reaches a fully developed icosahedral CN. Beyond CN, growth follows the icosahedral–dodecahedral dual motif with alternating shells, while additional \mathcal{I}_h -symmetric polyhedral motifs (at T7, T8, and T10) appear between neighboring icosahedral and dodecahedral shells to fill local voids and improve packing.

form around it (active regions highlighted at T6), resulting in a heterogeneous intermediate structure.

Crucially, the final symmetry emerges only at the late stages of growth. From T7 to the final C_2 nid-IQC state, atoms within the central C_6 -symmetric scaffold undergo a collective rearrangement that eliminates the symmetry mismatch with the surrounding shell, producing a defect-free, globally C_2 -

symmetric structure. Overall, unlike classical nucleation in which the CN templates the final symmetry, the symmetry-detour pathway is scaffolded by a C_6 -symmetric core that dynamically reorganizes to yield the final nid-IQC state.

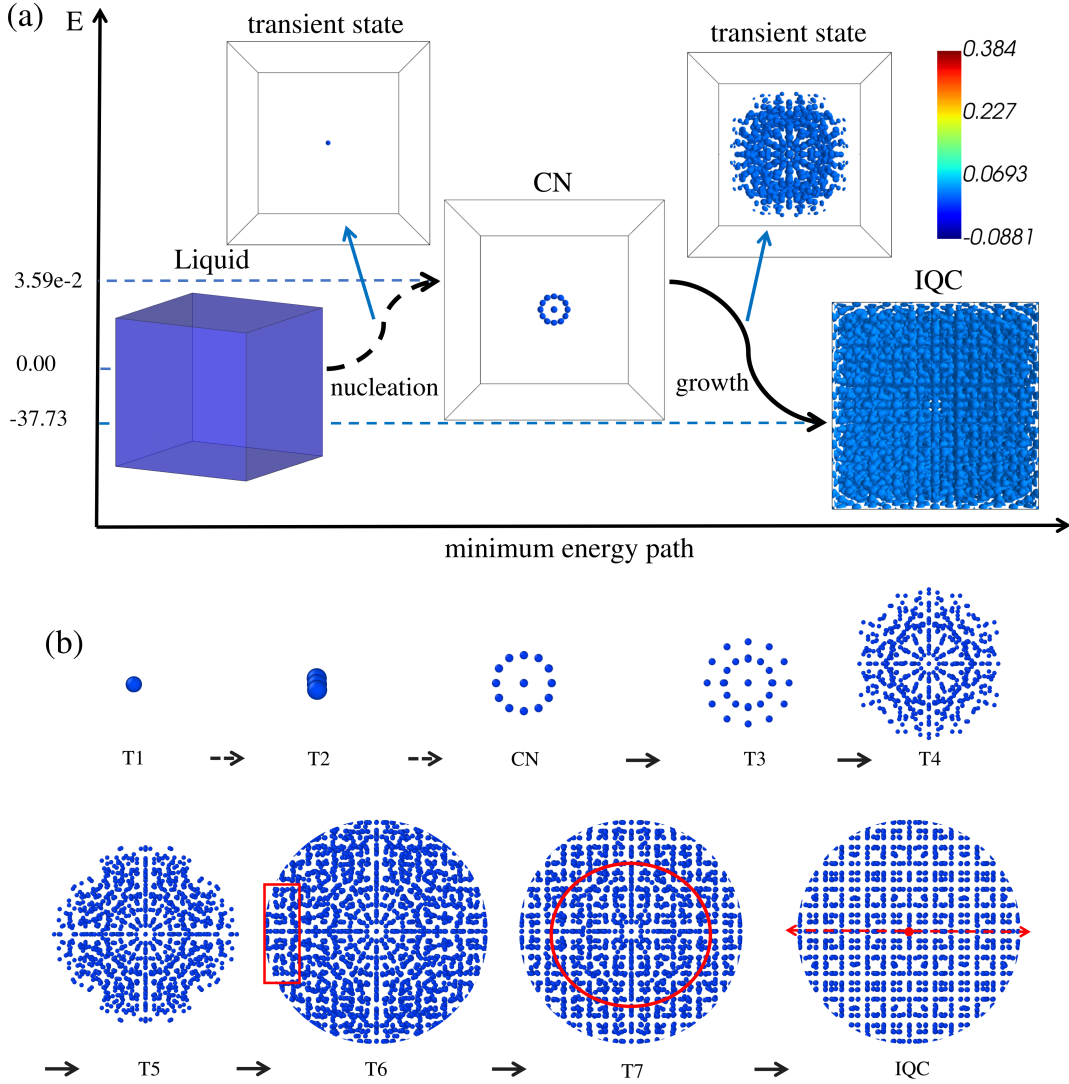


FIG. 7. **Nucleation and growth process of a representative nid-IQC along the MEP at $\varepsilon = 0.0861$ and $\alpha = 0.3$.** (a) Density profiles sampled along the MEP from the DIS to the nid-IQC, with the CN indicated. (b) Atomic configurations sampled along the MEP. The global symmetry follows a detour: DIS \rightarrow a CN with pronounced sixfold (C_6) features \rightarrow the C_2 -symmetric nid-IQC steady state. From CN to T6, the C_6 -symmetric nucleus acts as a temporary scaffold. Growth then proceeds via the progressive formation of characteristic local IQC clusters around this core (active regions marked by red rectangles). In the final stage (T6-IQC), atoms within the core rearrange to eliminate the symmetry mismatch, yielding the final C_2 -symmetric IQC.

VI. DISCUSSION

By combining a Landau free-energy model with the SPM, we identify nucleation pathways for IQCs. The essential difference from periodic crystals is the presence of phason degrees of freedom. Phason shifts generate a degenerate family of structurally distinct steady states and, already at nucleation, allow symmetry-distinct CNs with different barriers (Fig. 4).

For periodic crystals such as BCC, degeneracy arises solely from rigid translation. All translated states share identical symmetry and local coordination. Consequently, nucleation paths are translation-equivalent, and their CNs differ only by spatial position (Fig. 3). Increasing temperature simply scales

the barrier height without introducing new structural choices.

In contrast, IQC degeneracy originates from translations in a higher-dimensional embedding space. The parallel component β_{\parallel} corresponds to trivial rigid shifts, whereas the perpendicular component β_{\perp} (phasons) modifies the real-space symmetry. This generates a family of IQC steady states ranging from the \mathcal{I}_h -symmetric id-IQC to symmetry-broken nid-IQC variants. This phason-driven structural diversity naturally leads to multiple nucleation routes, yielding CNs with distinct symmetries (Fig. 4).

Temperature selects among these routes by reshaping the relative barrier heights (Fig. 4(e)). At low temperatures, the direct symmetry-preserving route toward the id-IQC is fa-

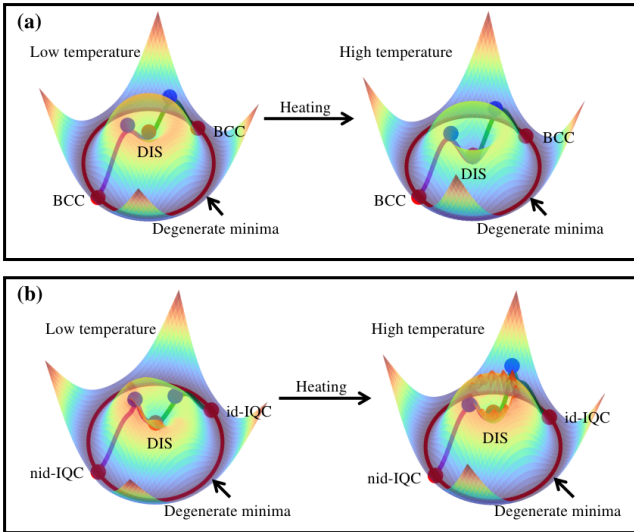


FIG. 8. Schematic energy landscapes for BCC and IQC nucleation. (a) BCC. Red circles denote degenerate BCC minima related by rigid translations in physical space. Blue dots denote the saddle points (CN). Representative nucleation pathways (green and purple) are translation-equivalent and therefore have identical barrier heights. Increasing temperature primarily raises the barrier without changing the pathway class. (b) IQC. Red circles denote thermodynamically degenerate IQC minima parameterized by higher-dimensional translations $\beta = \beta_{\parallel} + \beta_{\perp}$. Blue dots denote the corresponding saddle points. Two representative symmetry-distinct routes are illustrated, an id-IQC route (green) and a nid-IQC route (purple), whose relative barrier heights depend on temperature.

vored (Fig. 6). At higher temperatures, maintaining perfect \mathcal{I}_h symmetry in the CN incurs a steep energetic penalty from the quadratic cost of large-amplitude density modulations. The system then lowers the barrier by taking a symmetry detour via a lower-symmetry CN, leading to the nid-IQC (Fig. 7).

Taken together, our findings establish phasons as the structural origin of pathway diversity, providing a new physical picture for the emergence of quasiperiodic order (Fig. 8).

¹C. V. Achim, M. Schmiedeberg, and H. Löwen. Growth modes of quasicrystals. *Phys. Rev. Lett.*, 112:255501, 2014. doi:10.1103/PhysRevLett.112.255501.

²S. Alexander and J. McTague. Should all crystals be bcc? landau theory of solidification and crystal nucleation. *Phys. Rev. Lett.*, 41:702–705, Sep 1978. doi:10.1103/PhysRevLett.41.702. URL <https://link.aps.org/doi/10.1103/PhysRevLett.41.702>.

³Wooheyon Baek, Sambit Das, Shibo Tan, Vikram Gavini, and Wenhao Sun. Quasicrystal stability and nucleation kinetics from density functional theory. *Nature Physics*, 21(6):980–987, 06 2025. ISSN 1745-2481. doi:10.1038/s41567-025-02925-6. URL <https://doi.org/10.1038/s41567-025-02925-6>.

⁴Per Bak. Icosahedral crystals: Where are the atoms? *Phys. Rev. Lett.*, 56:861–864, Feb 1986. doi:10.1103/PhysRevLett.56.861. URL <https://link.aps.org/doi/10.1103/PhysRevLett.56.861>.

⁵Kobi Barkan, Haim Diamant, and Ron Lifshitz. Stability of quasicrystals composed of soft isotropic particles. *Phys. Rev. B*, 83:172201, May 2011. doi:10.1103/PhysRevB.83.172201. URL <https://link.aps.org/doi/10.1103/PhysRevB.83.172201>.

⁶Kobi Barkan, Michael Engel, and Ron Lifshitz. Controlled self-assembly of periodic and aperiodic cluster crystals. *Phys. Rev. Lett.*, 113:098304, Aug 2014. doi:10.1103/PhysRevLett.113.098304. URL <https://link.aps.org/doi/10.1103/PhysRevLett.113.098304>.

⁷Edwin A. Bedolla-Montiel, Susana Marín-Aguilar, and Marjolein Dijkstra. Relationship between structure and dynamics of an icosahedral quasicrystal using unsupervised machine learning. *The Journal of Chemical Physics*, 163(17):174503, 11 2025. ISSN 0021-9606. doi:10.1063/5.0292207. URL <https://doi.org/10.1063/5.0292207>.

⁸Jayanta K. Bhattacharjee and Kalyan Banerjee. Kramers time in bistable potentials. *J. Phys. A: Math. Gen.*, 22(24):L1141–L1146, dec 1989. doi:10.1088/0305-4470/22/24/002.

⁹Kurt Broderix, Kamal K. Bhattacharya, Andrea Cavagna, Annette Zippelius, and Irene Giardina. Energy landscape of a lennard-jones liquid: Statistics of stationary points. *Phys. Rev. Lett.*, 85:5360–5363, Dec 2000. doi:10.1103/PhysRevLett.85.5360. URL <https://link.aps.org/doi/10.1103/PhysRevLett.85.5360>.

¹⁰Gang Cui and Kai Jiang. Spring pair method of finding saddle points using the minimum energy path as a compass. *Phys. Rev. E*, 110:064123, Dec 2024. doi:10.1103/PhysRevE.110.064123. URL <https://link.aps.org/doi/10.1103/PhysRevE.110.064123>.

¹¹Gang Cui, Kai Jiang, and Tiejun Zhou. An efficient saddle search method for ordered phase transitions involving translational invariance. *Comput. Phys. Commun.*, 306:109381, 2025. ISSN 0010-4655. doi:<https://doi.org/10.1016/j.cpc.2024.109381>. URL <https://www.sciencedirect.com/science/article/pii/S0010465524003047>.

¹²Pablo F Damasceno, Sharon C Glotzer, and Michael Engel. Non-close-packed three-dimensional quasicrystals. *Journal of Physics: Condensed Matter*, 29(23):234005, may 2017. doi:10.1088/1361-648X/aa6cc1. URL <https://dx.doi.org/10.1088/1361-648X/aa6cc1>.

¹³Harold Davenport and Kurt Mahler. Simultaneous diophantine approximation. *Duke Math. J.*, 13(1):105–111, mar 1946. doi:10.1215/S0012-7094-46-01311-7.

¹⁴Marc de Boissieu. Phonons, phasons and atomic dynamics in quasicrystals. *Chem. Soc. Rev.*, 41:6778–6786, 2012. doi:10.1039/C2CS35212E. URL <http://dx.doi.org/10.1039/C2CS35212E>.

¹⁵Jim De Yoreo. More than one pathway. *Nature Materials*, 12(4):284–285, 04 2013. ISSN 1476-4660. doi:10.1038/nmat3604. URL <https://doi.org/10.1038/nmat3604>.

¹⁶Tomonari Dotera. Toward the discovery of new soft quasicrystals: From a numerical study viewpoint. *Journal of Polymer Science Part B: Polymer Physics*, 50(3):155–167, 2012. doi:<https://doi.org/10.1002/polb.22395>. URL <https://onlinelibrary.wiley.com/doi/abs/10.1002/polb.22395>.

¹⁷Jingshan S. Du, Yuna Bae, and James J. De Yoreo. Non-classical crystallization in soft and organic materials. 9(4):229–248, 04 2024. ISSN 2058-8437. doi:10.1038/s41578-023-00637-y. URL <https://doi.org/10.1038/s41578-023-00637-y>.

¹⁸Weinan E and Xiang Zhou. The gentlest ascent dynamics. *Nonlinearity*, 24(6):1831, may 2011. doi:10.1088/0951-7715/24/6/008. URL <https://dx.doi.org/10.1088/0951-7715/24/6/008>.

¹⁹Weinan E, Weiqing Ren, and Eric Vanden-Eijnden. String method for the study of rare events. *Phys. Rev. B*, 66:052301, Aug 2002. doi:10.1103/PhysRevB.66.052301. URL <https://link.aps.org/doi/10.1103/PhysRevB.66.052301>.

²⁰Michael Engel, Pablo F Damasceno, Carolyn L Phillips, and Sharon C Glotzer. Computational self-assembly of a one-component icosahedral quasicrystal. *Nature materials*, 14(1):109–116, January 2015. ISSN 1476-1122. doi:10.1038/nmat4152. URL <https://doi.org/10.1038/nmat4152>.

²¹Steffen Fischer, Alexander Exner, Kathrin Zielske, Jan Perlich, Sofia Deloudi, Walter Steurer, Peter Lindner, and Stephan Förster. Colloidal quasicrystals with 12-fold and 18-fold diffraction symmetry. *PNAS*, 108(5):1810–1814, 2011. doi:10.1073/pnas.1008695108.

²²B. Freedman, R. Lifshitz, J. W. Fleischer, and M. Segev. Phason dynamics in nonlinear photonic quasicrystals. *Nat. Mater.*, 6:776–781, 2007. doi:10.1038/nmat1981.

²³I. Han, K. L. Wang, A. T. Cadotte, Z. Xi, H. Parsamehr, X. Xiao, S. C. Glotzer, and A. J. Shahani. Formation of a single quasicrystal upon collision of multiple grains. *Nat. Commun.*, 12:5790, 2021. doi:10.1038/s41467-021-26070-9.

²⁴Z. He, J.-L. Maurice, H. Ma, Y. Wang, H. Li, T. Zhang, X. Ma, and

W. Steurer. Experimental observation of carousel-like phason flips in the decagonal quasicrystal $\text{Al}_{60}\text{Cr}_{20}\text{Fe}_{10}\text{Si}_{10}$. *Acta Crystallogr. Sect. A*, 77: 355–361, 2021. doi:10.1107/S2053273321003947.

²⁵Ted Janssen, Gervais Chapuis, and Marc de Boissieu. *Aperiodic Crystals: From Modulated Phases to Quasicrystals: Structure and Properties*. Oxford University Press, 06 2018. ISBN 9780198824442. doi:10.1093/oso/9780198824442.001.0001. URL <https://doi.org/10.1093/oso/9780198824442.001.0001>.

²⁶K. Je, S. Lee, E. G. Teich, M. Engel, and S. C. Glotzer. Entropic formation of a thermodynamically stable colloidal quasicrystal with negligible phason strain. *Proc. Natl. Acad. Sci. U.S.A.*, 118:e2011799118, 2021. doi:10.1073/pnas.2011799118.

²⁷Seung-Yeol Jeon, Hyungho Kwon, and Kahyun Hur. Intrinsic photonic wave localization in a three-dimensional icosahedral quasicrystal. *Nature Physics*, 13:363 – 368, 2017. URL <https://api.semanticscholar.org/CorpusID:126050476>.

²⁸Hyeong-Chai Jeong. Growing perfect decagonal quasicrystals by local rules. *Phys. Rev. Lett.*, 98:135501, Mar 2007.

²⁹Kai Jiang and Wei Si. Stability of three-dimensional icosahedral quasicrystals in multi-component systems. *Philosophical Magazine*, 100(1):84–109, 2020. doi:10.1080/14786435.2019.1671997. URL <https://doi.org/10.1080/14786435.2019.1671997>.

³⁰Kai Jiang and Pingwen Zhang. Numerical methods for quasicrystals. *Journal of Computational Physics*, 256:428–440, 2014. ISSN 0021-9991. doi:<https://doi.org/10.1016/j.jcp.2013.08.034>. URL <https://www.sciencedirect.com/science/article/pii/S002199911300572X>.

³¹Kai Jiang, Jiajun Tong, Pingwen Zhang, and An-Chang Shi. Stability of two-dimensional soft quasicrystals in systems with two length scales. *Phys. Rev. E*, 92:042159, Oct 2015. doi:10.1103/PhysRevE.92.042159. URL <https://link.aps.org/doi/10.1103/PhysRevE.92.042159>.

³²Kai Jiang, Pingwen Zhang, and An-Chang Shi. Stability of icosahedral quasicrystals in a simple model with two-length scales. *J. Phys.: Condens. Matter*, 29(12):124003, March 2017. ISSN 0953-8984. doi:10.1088/1361-648x/aa586b.

³³Kai Jiang, Shifeng Li, and Pingwen Zhang. Numerical methods and analysis of computing quasiperiodic systems. *SIAM Journal on Numerical Analysis*, 62(1):353–375, 2024. doi:10.1137/22M1524783. URL <https://doi.org/10.1137/22M1524783>.

³⁴Kai Jiang, Shifeng Li, and Pingwen Zhang. On the approximation of quasiperiodic functions with diophantine frequencies by periodic functions. *SIAM Journal on Mathematical Analysis*, 57(1):951–978, 2025. doi:10.1137/24M165925X. URL <https://doi.org/10.1137/24M165925X>.

³⁵S. Karthika, T. K. Radhakrishnan, and P. Kalaichelvi. A review of classical and nonclassical nucleation theories. *Crystal Growth & Design*, 16(11): 6663–6681, 2016. doi:10.1021/acs.cgd.6b00794. URL <https://doi.org/10.1021/acs.cgd.6b00794>.

³⁶Alexander Kiselev, Michael Engel, and Hans-Rainer Trebin. Confirmation of the random tiling hypothesis for a decagonal quasicrystal. *Phys. Rev. Lett.*, 109:225502, Nov 2012. doi:10.1103/PhysRevLett.109.225502. URL <https://link.aps.org/doi/10.1103/PhysRevLett.109.225502>.

³⁷Yaakov E. Kraus, Yoav Lahini, Zohar Ringel, Mor Verbin, and Oded Zilberg. Topological states and adiabatic pumping in quasicrystals. *Phys. Rev. Lett.*, 109:106402, Sep 2012. doi:10.1103/PhysRevLett.109.106402. URL <https://link.aps.org/doi/10.1103/PhysRevLett.109.106402>.

³⁸Ludwik Leibler. Theory of microphase separation in block copolymers. *Macromolecules*, 13(6):1602–1617, 1980. doi:10.1021/ma60078a047. URL <https://doi.org/10.1021/ma60078a047>.

³⁹Chu Li, Zhuo Liu, Eshani C. Goonetilleke, and Xuhui Huang. Temperature-dependent kinetic pathways of heterogeneous ice nucleation competing between classical and non-classical nucleation. *Nature Communications*, 12 (1):4954, 2021. ISSN 2041-1723. doi:10.1038/s41467-021-25267-2. URL <https://doi.org/10.1038/s41467-021-25267-2>.

⁴⁰Chaoping Liang, Kai Jiang, Sai Tang, Jincheng Wang, Yunzhu Ma, Wensheng Liu, and Yong Du. Molecular-level insights into the nucleation mechanism of one-component soft matter icosahedral quasicrystal studied by phase-field crystal simulations. *Cryst. Growth Des.*, 22(4):2637–2643, 2022. doi:10.1021/acs.cgd.2c00074. URL <https://doi.org/10.1021/acs.cgd.2c00074>.

⁴¹Ron Lifshitz. Symmetry breaking and order in the age of quasicrystals. *Israel Journal of Chemistry*, 51(11-12):1156–1167, 2011. doi:<https://doi.org/10.1002/ijch.201100156>. URL <https://onlinelibrary.wiley.com/doi/abs/10.1002/ijch.201100156>.

⁴²Ron Lifshitz and Dean M. Petrich. Theoretical model for faraday waves with multiple-frequency forcing. *Phys. Rev. Lett.*, 79:1261–1264, Aug 1997. doi:10.1103/PhysRevLett.79.1261. URL <https://link.aps.org/doi/10.1103/PhysRevLett.79.1261>.

⁴³James F. Lutsko. How crystals form: A theory of nucleation pathways. *Science Advances*, 5(4):eaav7399, 2019. doi:10.1126/sciadv.aav7399. URL <https://www.science.org/doi/abs/10.1126/sciadv.aav7399>.

⁴⁴Weining Man, Mischa Megens, Paul Steinhardt, and P Chaikin. Experimental measurement of the photonic properties of icosahedral quasicrystals. *Nature*, 436:993–6, 09 2005. doi:10.1038/nature03977.

⁴⁵Marek Mihalkovic, W. Zhu, C. Henley, and Mark Oxborrow. Icosahedral quasicrystal decoration models. i. geometrical principles. *Phys. Rev. B, Condensed matter*, 53:9002–9020, 05 1996. doi:10.1103/PhysRevB.53.9002.

⁴⁶Yuki Nagai, Yutaka Iwasaki, Koichi Kitahara, Yoshiki Takagiwa, Kaoru Kimura, and Motoyuki Shiga. High-temperature atomic diffusion and specific heat in quasicrystals. *Phys. Rev. Lett.*, 132:196301, May 2024. doi:10.1103/PhysRevLett.132.196301. URL <https://link.aps.org/doi/10.1103/PhysRevLett.132.196301>.

⁴⁷K. Nagao, T. Inuzuka, K. Nishimoto, and K. Edagawa. Experimental observation of quasicrystal growth. *Phys. Rev. Lett.*, 115:075501, 2015. doi:10.1103/PhysRevLett.115.075501.

⁴⁸Eva G. Noya and Jonathan P. K. Doye. A one-component patchy-particle icosahedral quasicrystal. *ACS Nano*, 19(14):13714–13722, 2025. doi:10.1021/acsnano.4c14885. URL <https://doi.org/10.1021/acsnano.4c14885>.

⁴⁹Eva G Noya, Chak Kui Wong, Pablo Llombart, and Jonathan P K Doye. How to design an icosahedral quasicrystal through directional bonding. *Nature*, 596(7872):367–371, August 2021. ISSN 0028-0836. doi:10.1038/s41586-021-03700-2. URL <https://digital.csic.es/bitstream/10261/256086/4/How%20to%20design%20an%20icosahedral%20quasicrystal.pdf>.

⁵⁰Diogo E. P. Pinto, Petr Šulc, Francesco Sciorino, and John Russo. Automating blueprints for the assembly of colloidal quasicrystal clusters. *ACS Nano*, 19(1):512–519, 2025. doi:10.1021/acsnano.4c10434. URL <https://doi.org/10.1021/acsnano.4c10434>.

⁵¹David A. Rabson, N. David Mermin, Daniel S. Rokhsar, and David C. Wright. The space groups of axial crystals and quasicrystals. *Rev. Mod. Phys.*, 63:699–733, Jul 1991. doi:10.1103/RevModPhys.63.699. URL <https://link.aps.org/doi/10.1103/RevModPhys.63.699>.

⁵²D. J. Ratliff, A. J. Archer, P. Subramanian, and A. M. Rucklidge. Which wave numbers determine the thermodynamic stability of soft matter quasicrystals? *Phys. Rev. Lett.*, 123:148004, Oct 2019.

⁵³D. S. Rokhsar, D. C. Wright, and N. D. Mermin. The two-dimensional quasicrystallographic space groups with rotational symmetries less than 23-fold. *Acta Crystallographica Section A*, 44(2):197–211, Mar 1988. doi:10.1107/S0108767387010511. URL <https://doi.org/10.1107/S0108767387010511>.

⁵⁴M. Schmiedeberg, C. V. Achim, J. Hielscher, S. C. Kapfer, and H. Löwen. Dislocation-free growth of quasicrystals from two seeds due to additional phasonic degrees of freedom. *Phys. Rev. E*, 96:012602, Jul 2017. doi:10.1103/PhysRevE.96.012602. URL <https://link.aps.org/doi/10.1103/PhysRevE.96.012602>.

⁵⁵Michael Schmiedeberg and Holger Stark. Colloidal ordering on a 2d quasicrystalline substrate. *Phys. Rev. Lett.*, 101(21):218302, November 2008. ISSN 0031-9007. doi:10.1103/physrevlett.101.218302. URL <https://doi.org/10.1103/PhysRevLett.101.218302>.

⁵⁶N. Senabulya and A. J. Shahani. Growth interactions between icosahedral quasicrystals. *Phys. Rev. Mater.*, 3:093403, 2019. doi:10.1103/PhysRevMaterials.3.093403.

⁵⁷D. Shechtman, I. Blech, D. Gratias, and J. W. Cahn. Metallic phase with long-range orientational order and no translational symmetry. *Phys. Rev. Lett.*, 53:1951–1953, Nov 1984. doi:10.1103/PhysRevLett.53.1951.

⁵⁸Paul J. M. Smeets, Aaron R. Finney, Wouter J. E. M. Habraken, Fabio Nudelman, Heiner Friedrich, Jozua Laven, James J. De Yoreo, P. Mark Rodger, and Nico A. J. M. Sommerdijk. A classical view on nonclassical nucleation. *Proceedings of the National Academy of Sciences*, 114

(38):E7882–E7890, 2017. doi:10.1073/pnas.1700342114. URL <https://www.pnas.org/doi/abs/10.1073/pnas.1700342114>.

⁵⁹J. E. S. Socolar, T. C. Lubensky, and P. J. Steinhardt. Phonons, phasons, and dislocations in quasicrystals. *Phys. Rev. B*, 34:3345–3360, 1986. doi:10.1103/PhysRevB.34.3345.

⁶⁰Gabriele C. Sosso, Ji Chen, Stephen J. Cox, Martin Fitzner, Philipp Pedevilla, Andrea Zen, and Angelos Michaelides. Crystal nucleation in liquids: Open questions and future challenges in molecular dynamics simulations. *Chemical Reviews*, 116(12):7078–7116, 2016. doi:10.1021/acs.chemrev.5b00744. URL <https://doi.org/10.1021/acs.chemrev.5b00744>. PMID: 27228560.

⁶¹P. Subramanian, A. J. Archer, E. Knobloch, and A. M. Rucklidge. Three-dimensional icosahedral phase field quasicrystal. *Phys. Rev. Lett.*, 117:075501, Aug 2016. doi:10.1103/PhysRevLett.117.075501.

⁶²Hiroyuki Takakura, Cesar Pay Gómez, Akiji Yamamoto, Marc De Boissieu, and An Pang Tsai. Atomic structure of the binary icosahedral Yb–Cd quasicrystal. *Nature Materials*, 6(1):58–63, 01 2007. ISSN 1476-4660. doi:10.1038/nmat1799. URL <https://doi.org/10.1038/nmat1799>.

⁶³Lei-Han Tang. Random-tiling quasicrystal in three dimensions. *Phys. Rev. Lett.*, 64:2390–2393, May 1990. doi:10.1103/PhysRevLett.64.2390. URL <https://link.aps.org/doi/10.1103/PhysRevLett.64.2390>.

⁶⁴José Urgel, David Écija, Guoqing Lyu, Ran Zhang, Carlos-Andres Palma, Willi Auwärter, Nian Lin, and Johannes Barth. Quasicrystallinity expressed in two-dimensional coordination networks. *Nature Chemistry*, 8, 05 2016.

⁶⁵Steurer Walter and Sofia Deloudi. *Crystallography of quasicrystals : concepts, methods and structures*. Crystallography of quasicrystals : concepts, methods and structures, 2009.

⁶⁶Kelly L. Wang, Insung Han, Domagoj Fijan, Sharon C. Glotzer, and Ashwin J. Shahani. Defect-free growth of decagonal quasicrystals around obstacles. *Phys. Rev. Lett.*, 135:166203, Oct 2025. doi:10.1103/bsbs-rryl. URL <https://link.aps.org/doi/10.1103/bsbs-rryl>.

⁶⁷M. Widom. Discussion of phasons in quasicrystals and their dynamics. *Philos. Mag.*, 88:2339–2350, 2008. doi:10.1080/14786430802247163.

⁶⁸Ke-Jun Wu, Edmund C.M. Tse, Congxiao Shang, and Zhengxiao Guo. Nucleation and growth in solution synthesis of nanostructures – from fundamentals to advanced applications. *Progress in Materials Science*, 123:100821, 2022. ISSN 0079-6425. doi: <https://doi.org/10.1016/j.pmatsci.2021.100821>. URL <https://www.sciencedirect.com/science/article/pii/S0079642521000451>. A Festschrift in Honor of Brian Cantor.

⁶⁹T. Yamada, H. Takakura, H. Euchner, C. Pay Gómez, A. Bosak, P. Fertey, and M. De Boissieu. Atomic structure and phason modes of the Sc–Zn icosahedral quasicrystal. *IUCrJ*, 3:247–258, 2016. doi:10.1107/S2052252516007041.

⁷⁰J. Yin, L. Zhang, and P. Zhang. Transition pathways connecting crystals and quasicrystals. *Proc. Natl. Acad. Sci. U.S.A.*, 118:e2106230118, 2021. doi:10.1073/pnas.2106230118.

⁷¹Cui Gang Jiang Kai Shi An-Chang Zhang Pingwen Yin Jianyuan Zhang, Zhiyi and Lei Zhang. Exploring transition pathways in the landau-brazovskii model. *Phys. Rev. Res.*, pages –, Jan 2026. doi:10.1103/q4gq-dkkp. URL <https://link.aps.org/doi/10.1103/q4gq-dkkp>.

⁷²T. Zhou, L. Zhang, P. Zhang, A.-C. Shi, and K. Jiang. Nucleation and phase transition of decagonal quasicrystals. *J. Chem. Phys.*, 161:164503, 2024. doi:10.1063/5.0232334.

⁷³Oded Zilberberg, Sheng Huang, Jonathan Guglielmon, Mohan Wang, Kevin P. Chen, Yaakov E. Kraus, and Mikael C. Rechtsman. Photonic topological boundary pumping as a probe of 4d quantum hall physics. *Nature*, 553(7686):59–62, 2018. ISSN 1476-4687. doi:10.1038/nature25011. URL <https://doi.org/10.1038/nature25011>.